Journal of Drug Delivery Science and Technology 124 (2026) 108648

Contents lists available at ScienceDirect

Journal of Drug Delivery Science and Technology

journal homepage: www.elsevier.com/locate/jddst

Ellagic acid-loaded galactosylated liposomes: an efficient strategy for counteracting senescence in mixed primary glial cells

Elisa Landucci [a], Rebecca Castellacci [b,1], Alba Puente-Sanz [a,1], Costanza Mazzantini [a], Domenico E. Pellegrini-Giampietro [a], Anna Rita Bilia [b], Maria Camilla Bergonzi [b,*]

[a] Department of Health Sciences, Section of Clinical Pharmacology and Oncology, University of Florence, Florence, Italy
[b] Department of Chemistry "Ugo Schiff", University of Florence, Via Ugo Schiff 6, Sesto Fiorentino, Florence, 50019, Italy

ARTICLE INFO

Keywords:
Ellagic acid
Galactosylated liposomes
Nanocarrier targeting
BBB-PAMPA
Mixed glial cells
Doxorubicin
Senescence therapy

ABSTRACT

Aging constitutes a multifaceted biological phenomenon with profound implications for the central nervous system. Astrocytes, which serve as vital homeostatic support cells, undergo a transition toward cellular senescence over time, thereby fueling the progression of neurodegenerative pathologies. Ellagic acid (EA) is a natural polyphenol present in various fruits and nuts that has recently garnered attention for its potential anti-aging and anti-senescence properties. It has beneficial effects in models of neurodegeneration, cardiovascular and renal aging, and oxidative stress. However, its clinical application is hindered by low water solubility, poor stability, low permeability, and limited bioavailability.

To overcome these shortcomings and optimize its efficacy, galactosylated liposomes using galactosylceramide (Gal-LP-EA) were optimized. Liposomal encapsulation improved the water solubility of EA and they exhibited high encapsulation efficiency, good stability in the presence of human serum albumin and storage stability, and slow drug release profile. Gal-LP-EA improved EA permeability coefficient in BBB-PAMPA assay.

The ability of EA and Gal-LP-EA to counteract the senescence induced by doxorubicin was analysed in mixed primary glial cells. The results demonstrated that doxorubicin treatment induced a senescent phenotype in mixed glial cells, characterized by increased expression of senescence markers such as p21 and by decrease of Ki67 and SIRT1 along with activation of the DNA damage response (γ-H2AX and p53). Also, EA and especially Gal-LP-EA were able to reduce this effect.

The results of this multidisciplinary study underscore the potential of developing EA-loaded galactosyl-coated liposomes to modulate pathways involved in age-related neurodegeneration.

1. Introduction

Cellular senescence is a stable state of cell-cycle arrest characterized by persistent metabolic activity, resistance to apoptosis, chromatin remodeling, and the acquisition of a pro-inflammatory secretory phenotype known as the senescence-associated secretory phenotype (SASP) [1]. Initially described as a tumor-suppressive mechanism limiting the proliferation of damaged cells, senescence is now recognized as a complex biological process with both physiological and pathological roles [2]. Physiologically, transient senescence contributes to tissue remodeling, embryonic development, and wound healing. However, when senescent cells accumulate chronically, they promote tissue dysfunction, inflammation, and age-related pathologies. Accumulating evidence indicates that cellular senescence is a fundamental contributor to the pathogenesis of numerous age-associated disorders, including neurodegenerative diseases, cancer, metabolic dysfunction, cardiovascular disease, and chronic inflammatory conditions [2,3].

Several antineoplastic agents, including the anthracycline doxorubicin, induce senescence through persistent DNA damage and activation of the DNA damage response (DDR). The DDR is initiated by the recruitment of sensor complexes to damaged chromatin, followed by activation of the ATM/ATR kinases and phosphorylation of downstream substrates, including histone H2AX (γH2AX) and the tumor suppressor p53. Upon stabilization, p53 undergoes post-translational modifications such as acetylation, which enhance its transcriptional activity toward

* Corresponding author.
E-mail address: mc.bergonzi@unifi.it (M.C. Bergonzi).
[1] These authors contributed equally to this study.

https://doi.org/10.1016/j.jddst.2026.108648
Received 10 April 2026; Received in revised form 23 June 2026; Accepted 25 June 2026
Available online 25 June 2026

cell-cycle inhibitors, most notably p21. Increased p21 expression inhibits cyclin-dependent kinases and enforces stable cell-cycle arrest. Importantly, the NAD^+-dependent deacetylase SIRT1 acts as a negative regulator of this pathway by deacetylating p53 and limiting its transcriptional activity. Reduced SIRT1 expression therefore facilitates sustained p53 signaling and contributes to consolidation of the senescent phenotype [4–6].

Evidence of doxorubicin-induced senescence has been widely reported in tumor cells [7], endothelial cells [8], fibroblasts [9], cardiomyocytes [10], and neural progenitors [11], highlighting its broad impact across cell types.

Glial cells play essential roles in maintaining neuronal homeostasis, regulating synaptic function, supporting metabolic coupling, and orchestrating immune responses [12]. Astrocytes and microglia are particularly sensitive to genotoxic and oxidative stress, and accumulating evidence indicates that both cell types can acquire a senescent phenotype during aging and neurodegenerative diseases such as Alzheimer's disease and Parkinson's diseases [12,13]. While most *in vitro* studies rely on isolated astrocyte cultures, mixed glial cultures provide a more physiologically relevant environment by preserving intercellular crosstalk and paracrine signaling. This is especially relevant in the context of senescence, where SASP factors and inflammatory mediators can induce secondary senescence in neighboring cells through paracrine signaling mechanisms, thereby amplifying tissue-level dysfunction [14]. Therefore, mixed glial cultures may better recapitulate the multicellular dynamics occurring in the aging brain.

EA is a natural polyphenol that has recently garnered attention for its potential anti-aging and anti-senescence properties [15]. Its beneficial effects in models of neurodegeneration, cardiovascular and renal aging, and oxidative stress have been widely reported [16,17]. However, its clinical application is hindered by low water solubility (9.7 μg/mL) [18], poor stability, and limited bioavailability. Additionally, EA exhibits poor permeability, as demonstrated by permeability coefficient (Pe) value of 2.2×10^{-7} cm/s across the blood-brain barrier (BBB) [19]. To overcome these limitations, liposomal formulations have emerged as a promising strategy to improve EA therapeutic performance. Khan et al. showed that liposomal EA improved antifungal efficacy and reduced systemic toxicity in a cyclophosphamide-induced leukopenic murine model of systemic *Cryptococcus neoformans* infection compared with free EA and fluconazole [20].

Emerging evidence indicates that EA can modulate key cellular stress pathways implicated in senescence, including oxidative stress, inflammation, autophagy, and DNA damage signaling. In human dermal fibroblasts subjected to oxidative stress, EA has been shown to attenuate markers of senescence such as senescence-associated β-galactosidase (β-gal) activity and DNA damage (γH2AX and p53), while restoring cell viability and cell cycle progression, and suppress pro-inflammatory cytokines by enhancing antioxidant defenses Collectively, these findings support the rationale for investigating EA as a candidate modulator of cellular senescence. Despite the increasing recognition of senescence in aging, chemotherapy-related neurotoxicity and neurodegenerative diseases, effective strategies to modulate or prevent senescence, specifically in glial cells, remain limited. Moreover, improving the bioavailability and targeted delivery of therapeutic agents represents a critical challenge.

The overexpression of the enzyme β-gal represents a functional and targetable enzymatic hallmark of senescent cells. β-gal is capable of specifically recognizing and processing galactose-containing substrates [21]. From a pharmaceutical technology perspective, this enzymatic activity provides a valuable opportunity to design enzyme-responsive nanocarriers able to selectively interact with β-gal-enriched cellular environments. Among galactose-containing substrates, galactosylceramide (Gal) has been reported in the literature as a promising targeting moiety [22,23].

In the present study, Gal was employed as a β-gal-responsive functional lipid to develop galactosylated liposomes encapsulating EA to improve its solubility, stability, permeability and pharmacological effects. The underlying rationale is that enzyme-mediated recognition at the nanocarrier surface may enhance selective uptake by senescent cells and potentially promote the intracellular release of the encapsulated active compound. Galactosyl-functionalized formulations have been proposed to enhance cellular uptake and potentially increase drug effectiveness [22,24,25]. However, whether galactosyl-decorated formulations improve therapeutic efficacy in the context of chemotherapy-induced glial senescence has not been thoroughly explored.

In this study, a preclinical *in vitro* model of chemotherapy-induced senescence in mixed glial cultures was established using doxorubicin. The aim of this study was to evaluate whether galactosyl-coated liposomes enhance EA solubility, permeability and biological efficacy. Ultimately, this study seeks to provide mechanistic insights into glial senescence and to explore novel delivery strategies for mitigating senescence processes.

2. Materials and methods

2.1. Chemicals and reagents

Ellagic acid (EA) with 98% purity, cholesterol ≥95% (CH), acetonitrile (HPLC grade), dichloromethane, methanol (HPLC grade), formic acid (analytical grade), phosphate-buffered saline (PBS, pH 7.4), ethanol (96%), dodecane (≥99%), Coumarin 6 (6C, purity 98%) and Human Serum Albumin (HSA) were sourced from Sigma Aldrich (Milan, Italy). Phosphatidylcholine (Phospholipon 90G, P90G) was obtained from Lipoid AG (Cologne, Germany). Ultrapure water was prepared using the Merck Millipore Simplicity® UV Water Purification System (Merck KGaA, Darmstadt, Germany). Galactosylceramide (Gal) was supplied by Cayman Chemical Company (Ann Arbor, Michigan, USA). Porcine polar brain lipid (PBL) was purchased from Avanti Polar Lipids, Inc. (Alabaster, AL).

2.2. Analytical method

EA quali-quantitative analyses were performed using a High-Performance Liquid Chromatograph (HPLC), HP 1200, equipped with an autosampler and a Diode Array Detector (DAD), (Agilent Technology, Santa Clara, CA, USA). The column was a Kinetex C18 (150 × 4.6 mm, 5 μm) maintained at 25 °C. A gradient analytical method with 0.8 mL/min flow rate was applied, using (A) acetonitrile and (B) formic acid/water pH 3.2 as mobile phase. The gradient profile was: 0–8 min, 5% A, 95% B; 8–12 min, 5-40% A, 95-60% B; 12–13 min, 40-5% A, 60–95% B; 13–20 min, 5–5% A, 95–95% B to re-equilibrate the column at the start of the method. The UV spectra were acquired at 254 nm with a retention time of approximately 8.2 min. A calibration curve was obtained preparing a stock solution of EA in MeOH (0.35 mg/mL) subsequently diluted with MeOH 5, 10, 100-folds and injected (10, 20, 30 μL for each dilution). The linear correlation coefficient R^2 was 0.9999.

The quali-quantitative determination of 6C was performed using a Supelco analytical column (25 cm × 4.6 mm, 5 μm). The chromatographic analysis was carried out at a flow rate of 1 mL/min using acetonitrile and formic acid/water solution (pH 3.2) as mobile phases under isocratic elution conditions (95% acetonitrile and 5% aqueous phase). UV detection was performed at 444 nm. The stock solution (6C 0.105 mg/mL in MeOH) was diluted 1, 2, 10 and 20-fold to obtain the calibration standards. The calibration curve showed a correlation coefficient (R^2) of 0.9999.

2.3. Preparation of EA-loaded galactosylceramide-coated liposomes (Gal-LP-EA)

Gal-LP-EA were prepared by the thin-film hydration technique, as previously described [26]. Briefly, 200 mg of P90G, CH, and Gal at a

gravimetric ratio of 7:2.5:0.5 were dissolved together with 5 mg of EA in 12 mL of a 1:1 (v/v) dichloromethane/methanol mixture. The system was sonicated for 1 min and subsequently maintained at 37 °C under magnetic stirring for 10 min to promote complete EA solubilization in the organic phase [27,28]. Afterward, the organic solvent was removed under vacuum evaporation, leading to the formation of the thin lipid film. The film was hydrated with 10 mL of deionized water and mechanically stirred at 50 °C for 30 min. Size reduction and sample homogenization were achieved by probe sonication for 4 min (2 s on/off cycles, 46% amplitude), while keeping the dispersion in an ice bath to avoid lipid degradation.

Empty liposomes (Gal-LP) were prepared according to the same procedure.

2.4. Preparation of 6C-Loaded galactosylceramide-coated liposomes (Gal-LP-6C)

Gal-LP-6C were prepared following the same procedure described for Gal-LP-EA. Briefly, 2 mg of 6C were dissolved in the lipid phase, obtaining a final concentration of 0.2 mg/mL.

2.5. Physical and chemical characterization

The physical characterization of liposomal formulations was carried out using a Zeta Sizer Pro instrument (Malvern Instruments Ltd.; Worcestershire, UK). Particle size (nm), polydispersity index (PdI), and Zeta potential (mV) were determined by Dynamic Light Scattering (DLS) and Electrophoretic Light Scattering (ELS) analyses, following a 10-fold dilution of the samples with deionized water.

Chemical characterization was performed by determining the encapsulation efficiency (EE%) through the direct dialysis bag method, as described by Ref. [29]. Regenerated cellulose dialysis membranes (Spectrum Laboratories, Inc., Breda, The Netherlands; MWCO 12–14 kDa) were employed. Briefly, 2 mL of liposomal formulations were placed into the dialysis bag, which was subsequently immersed in 1 L of Millipore water and maintained under continuous magnetic stirring for 1 h at room temperature (25 °C). After purification, 100 μL of the dialyzed sample were mixed with 900 μL of methanol. The resulting solution was sonicated in an ultrasonic bath for 30 min to ensure complete disruption of the nanocarrier system, followed by ultracentrifugation at 14,000 rpm for 10 min. The obtained supernatant was finally analysed by HPLC-DAD, and the EE% was calculated according to the following equation (1) [30]:

$$EE\% = \frac{weight\ of\ EA\ in\ liposomes}{weight\ of\ AE\ fed} x100 \quad (1)$$

2.6. Stability studies

The physical and chemical stability of Gal-LP-EA was evaluated over a 30-day period under refrigerated conditions (+4 °C). At predetermined time intervals, the formulations were analysed in terms of particle size, PdI, and Zeta potential. In parallel, chemical stability was assessed by monitoring variations in EE%.

To mimic physiological conditions, the Gal-LP-EA was incubated in an HSA solution prepared in PBS at a concentration of 45 mg/mL. This concentration falls within the physiological range of albumin in human blood plasma (35-50 g/L). Specifically, 200 μL of Gal-LP-EA dispersion was mixed with 2 mL of the HSA solution and incubated for 3 h, following established protocols [30,31]. The stability of the formulation under blood-mimicking conditions was subsequently evaluated by measuring particle size and PdI at selected time points. Prior to DLS analysis, samples were diluted four-fold with ultrapure water.

2.7. In vitro drug release study

Dialysis bag technique, employing regenerated cellulose dialysis membranes (Spectrum Laboratories, Inc., Breda, The Netherlands; MWCO 12–14 kDa) was used for *in vitro* release study [32]. EA-solution (0.33 mg/mL in methanol) and 2 mL of Gal-LP-EA (0.5 mg/mL) were loaded into a pre-hydrated dialysis bag, which was subsequently placed in a beaker containing 100 mL of a PBS/EtOH mixture (70:30, v/v) used as the release medium. The system was maintained at 37 °C throughout the experiment under continuous magnetic stirring at 100 rpm.

At predetermined time points, 1 mL aliquots of the release medium were collected. To preserve sink conditions, each withdrawn sample was immediately replaced with an equal volume of fresh PBS/EtOH solution. The collected samples were analysed by HPLC-DAD to quantify the amount of EA released over a 48 h period. The cumulative percentage of EA released was calculated according to the following equation (2):

$$\%\ Release = \frac{\frac{\mu g}{\mu l\ injected} x\ Vtot\ medium}{Cformulation\ x\ Vformulation\ in\ bag} \quad (2)$$

2.8. Parallel artificial membrane permeability Assay (PAMPA)

The BBB-PAMPA assay was employed to estimate the passive permeability of EA across a membrane miming the BBB, using a 96-well MultiScreen-IP filter plate (Millipore Corporation, Tullagreen, Carrigtwohill, Cork, Ireland).

To reproduce the lipidic composition of the BBB, the artificial membranes were coated with 10 μL PBL solution (2% w/v in n-dodecane) [33]. The donor compartment was then loaded with 250 μL of EA solution (0.3 mg/mL in methanol, diluted with PBS to a final concentration of 0.1 mg/mL) or Gal-LP-EA dispersion (0.5 mg/mL), while the acceptor compartment was filled with 250 μL of PBS/EtOH (70:30, v/v). The assay was carried out at room temperature (25 °C).

After assembling the PAMPA sandwich, samples were collected from the acceptor compartment at 4, 8, and 17 h. The withdrawn samples were appropriately diluted with methanol, subjected to ultrasonic bath treatment for 30 min to ensure complete disruption of the formulation, and subsequently ultracentrifuged at 14,000 rpm for 10 min. The resulting supernatants were analysed by HPLC-DAD to quantify EA concentration.

The effective permeability coefficient (Pe), expressed in cm^2/s, was calculated according to the following equation (3):

$$Pe = C \cdot \left[-ln\left(1 - \frac{Ca}{Cequilibrium}\right)\right] \quad (3)$$

Where:

$$C = \frac{(Vd \cdot Va)}{[(Vd + Va) \cdot A \cdot t]} \quad (4)$$

$$Cequilibrium = \frac{[Cd \cdot Vd + Ca \cdot Va]}{Vd + Va} \quad (5)$$

A represents the filter surface area (0.24 cm^2) multiplied by the apparent porosity of the filter (f), which is 20% or 0.048 cm^2. V_a and V_d represent the acceptor volume (250 μL) and the donor volume (250 μL), respectively. t is the incubation time (in seconds), while C_a and C_d refer to the drug concentrations in the acceptor (mg/mL) and donor (mg/mL) compartments, respectively.

2.9. Cellular study

2.9.1. Animals

Wistar rats (Charles River, Italy) were used for the preparation of primary cultures of mixed glial cells. All animal experiments satisfied the regulatory requirements of the European Parliament (Directive 2010/63/EU), European Union Council (September 22, 2010), and

Italian Animal Welfare Law (DL 26/2014). The protocol received approval from the Institutional Animal Care and Use Committee (Univ. Florence) and the Italian Ministry of Health. Animal suffering and the animal number required for data reproducibility were minimized.

2.9.2. Mixed rat glial cells

Primary mixed cultures of astrocytes and microglia (referred as "mixed glial cells") were prepared from post-natal day 1-2 Wistar rats as previously described [34,35] and grown in DMEM (Dulbecco's Modified Eagle's Medium – high glucose DMEM D6546-500 ML, Merck Life Science, Milan, Italy) +10% fetal bovine serum (FBS) (Honduras Origin F7524, Merck Life Science, Milan, Italy). Briefly, cortices were isolated in cold phosphate-buffered saline (PBS) and then incubated for 10 min at 37 °C in phosphate-buffered saline containing 0.25% trypsin (Trypsin-EDTA Solution T3924-100 ML, Merck Life Science, Milan, Italy) and 0.05% DNase (Deoxyribonuclease I from bovine pancreas DN25-100 MG, Merck Life Science, Milan, Italy). After blocking enzymatic digestion with the addition of 10% heat-inactivated FBS, cortices were mechanically disrupted, washed, and the cells resuspended in DMEM+10% FBS and plated in 24-well plates. The cells after they had reached the confluence were stimulated with 250 nM doxorubicin (D1515 Merck Life Science, Milan, Italy). The dose of doxorubicin was selected by the literature [36,37]. EA was dissolved in dimethyl sulfoxide (4 mg/mL), and was stored at −20 ∘C. For the experiments, EA was diluted in cell culture medium. EA and Gal-LP-EA were added to the culture medium together with doxorubicin. Cells were lysed after 24 h of exposure for real-time PCR and for Western Blot assays. Cultures were kept in an incubator at 37 °C, 100% humidity, and 95% air/5% CO2 atmosphere and used for experiments at 7-8 days *in vitro*.

2.9.3. Lactate dehydrogenase (LDH) assay

Cytotoxicity after drugs exposure was verified with the LDH assay. Damage in mixed glial cells was quantitatively assessed by measuring the amount of LDH released by the damaged cells into the culture medium, 24 h and 4 days after ellagic acid or liposomes alone or in combination with doxorubicin exposure, by adding catalyst and dye solutions of a Cytotoxicity Detection Kit (LDH) (Roche Diagnostics, Indianapolis, IN). The absorbance values were recorded at 490 nm and 690 nm. Cytotoxicity was expressed as a percentage compared to the maximum LDH release in the presence of Triton X-100 (TX).

2.9.4. 3-(4,5-dimethylthiazol-2-yl)-2,5-diphenyltetrazolium bromide (MTT) assay

To assess cell viability after drugs exposure, the MTT assay was performed in mixed glial cells. 24 h and 4 days after the end of treatments with EA or Gal-LP-EA alone or in combination with doxorubicin, cells were treated with 1 mg/mL of MTT for 15 min at 37 °C and 5% CO2. Finally, DMSO was added to dissolve MTT formation, and absorbance was measured at 550 and 690 nm. Cell viability was expressed as a percentage compared to CRL. Triton X-100 was employed as the negative control since its detergent action disrupts the cells.

2.9.5. Quantitative real-time polymerase chain reaction (RT-qPCR)

Evaluation of p53, cyclin-dependent kinase inhibitor 1A (p21) and Sirtuin 1 (SIRT1) Gene Expression by Quantitative Real-Time Polymerase Chain Reaction (RT-qPCR). Total RNA was isolated from mixed glial cells using Trizol Reagent REF #15596026 (Thermo Fisher Scientific, Milan, Italy). One μg of RNA was retrotranscribed using PrimeScript RT Reagent Kit with Gdna Eraser (Perfect Real Time 100 Rxns #RR047A, Diatech Lab Line Srl, Jesi,AN, Italy). RT-qPCR was performed as reported (Primers were purchased from Integrated DNA Technologies (Iowa, USA). Ribosomal 18S RNA was used as the normalizer. Quantitative PCR was performed using the following procedure: 95 °C for 30 s, 95 °C for 5 s and 60 °C for 15 s for 45 cycles. The sequences of the primers used read as follows: P53 rat forward 5' - TGCAGAGTTGTTAGAAGGCCCAGAGG - 3′ reverse 5' - ACTTGGCTGTCCCTGACTGCAGGAA - 3'; P21 rat forward 5' – TCCGATCCTGGTGATGTCCGACC - 3′ reverse 5' – GAACACGCTCCCAGACGTAGTTGC - 3'; SIRT1 rat forward 5' - TCTCCCAGATCCTCAAGC CATGTTCG - 3′ reverse 5' - AAAATTGCTTTCCTTCCACTGCACAGGC - 3'; 18S rat forward 5′- GGCGGCTTTGGTGACTCTAGATAACC -3′ and reverse 5′- CCTGCTGCCTTCCTTGGATGTGG -3'.

2.9.6. Western blotting

Evaluation of Ki67 and anti-phospho-Histone H2AX (γ-H2AX) protein expression by Western Blotting. Mixed glial cells were washed with cold 0.01 M PBS, pH 7.4, at the end of the treatment and dissolved in 1% SDS. The BCA (bicinchoninic acid) protein assay was used to quantify the total protein levels. Lysates (20 μg/lane of protein) were resolved by electrophoresis on a 4–20% SDS-polyacrylamide gel (Bio-Rad Laboratories, Hercules, CA) and transferred onto nitrocellulose membranes. After, the membranes (Bio-Rad, Milan, Italy; Cat. Nos. 1704158 and 1704159) were blocked for 5 min using EveryBlot® Blocking Buffer (Bio-Rad, Milan, Italy; Cat. No. 12010020). Then, the membranes were incubated overnight at 4 °C with rabbit polyclonal antibodies against Ki-67 (PA5-143612) (from Invitrogen, Life Technologies, Segrate, Milan, Italy), polyclonal rabbit antibodies against Phospho-Histone H2A.X (Ser139) (2577) (Cell Signaling Technology, Beverly, MA), diluted 1:1000 in TBS-T containing 5% bovine serum albumin. As a loading control, the monoclonal anti-β-actin antibody was from Sigma (St. Louis, MO). Immunodetection was performed with secondary antibodies (1:3000 anti-mouse or antirabbit IgG from donkey, Amersham Biosciences, Amersham, UK) conjugated to horseradish peroxidase in TBS-T containing 5% non-fat dry milk. Membranes were washed with TBS-T, and then reactive bands were detected using chemiluminescence (ECL-plus; Euroclone, Padova, Italy). Quantitative analysis was performed using the QuantityOne analysis software (Bio-Rad, Hercules, CA).

2.9.7. SA-β-gal staining for senescence detection

Senescence-associated β-galactosidase (SA-β-gal) activity was qualitatively assessed using the Senescence β-Galactosidase Staining Kit (Ref# 9860, Cell Signaling Technology, Baverly, MA, EEUU) according to the manufacturer's instructions. Briefly, cells were washed with PBS and fixed with Fixative Solution, followed by two additional PBS washes. The β-galactosidase staining solution was freshly prepared to obtain a final pH of 6.0. Cells were incubated with the staining solution at 37 °C overnight in a dry incubator without CO_2 to prevent pH fluctuations. Senescent cells were identified by the development of a blue precipitate under bright-field microscopy (200× magnification). For quantitative analysis, SA-β-gal-positive cells were identified by the presence of blue cytoplasmic staining and expressed as a percentage of the total number of cells within each field. Data were quantified using the Threshold Color plugin in ImageJ software (National Institutes of Health, Bethesda, MD, USA) and expressed as the percentage of SA-β-gal-positive cells.

2.9.8. Cellular uptake studies

For the evaluation of the intracellular content of 6C, mixed glial cells were cultured on histological slides and were exposed for 1 h to Gal-LP-6C loaded with 0.2 mg/mL of 6C and diluted 1: 40 into a medium, and to a solution of fluorescent probe at the final concentration of 5 μg/mL of 6C. At the end of the treatment, cells were fixed in 4% formaldehyde in phosphate buffer 0.1 mol/L, pH 7.4, for 15 min and stained with DAPI shielded fluorine (Sigma, Milan, Italy) to visualize the nucleus. Cellular uptake was studied by fluorescence microscopy using 6C-labeled liposomes, with a high-pressure mercury vapor lamp, 20× objective (OLYMPUS BX3-CBH/U-MCZ, Evident Europe GmbH, Milan, Italy). Filter set: excitation 365 nm emission 400 nm high pass DAPI, excitation 485 nm emission 524 nm. Fluorescence intensity was calculated with ImageJ software and was normalized to the cell number in each field.

2.9.9. Statistical analysis

Data are expressed as mean ± standard deviation (SD). For cellular

studies, the statistical significance of differences between control and treatment groups in LDH and MTT assay was analysed using one-way ANOVA followed by a post hoc Dunnett's test for multiple comparisons. One-way ANOVA followed by post hoc Tukey test for multiple comparisons were used for analyzing gene and protein expression levels and for SA-β-Gal activity. Cellular uptake studies of 6C and Gal-LP-6C were analysed using Student's t-test. GraphPad Prism v. 8 for Windows (GraphPad Software, San Diego, CA) was used to perform all statistical analyses, considering a probability value (p) < 0.05 as significant.

3. Results and discussion

3.1. Preparation and chemical-physical characterization of Gal-LP-EA

The increase in life expectancy and the growing aging population have led to a rise in chronic and degenerative diseases [38]. A common hallmark of these conditions is cellular senescence, a state of irreversible cell cycle arrest that contributes to tissue dysfunction [39]. Unlike quiescent cells, senescent cells are metabolically active and secrete pro-inflammatory and pro-oxidant molecules, collectively known as the SASP, which fosters chronic inflammation and disease progression [40]. Senescent cells exhibit increased size, mitochondrial dysfunction, lysosomal accumulation, and the formation of senescence-associated heterochromatin foci (SAHFs); however, no universal markers exist [41]. Common indicators include upregulation of the cell cycle inhibitors p16INK4a, p21CIP1 and p27. Notably, the overexpression of the enzyme β-Gal is a widely used marker [42] and it represents the investigated strategy of this study. EA is a polyphenolic compound primarily found in *Punica granatum* L., though it is also present in blueberries, strawberries, grapes, walnuts, and almonds [43]. EA reduces ROS, lipid peroxidation, and inflammatory mediators such as TNF-α, while increasing endogenous antioxidant levels including GSH and CAT. Despite its numerous beneficial effects, the therapeutic use of EA is limited due to its low solubility and poor bioavailability in an aqueous environment. To overcome these limitations, nanotechnology-based drug delivery systems have gained significant attention [44]. EA-loaded nanocarriers, including nanoparticles [45–47], polymeric micelles [48], and liposomes [49,50] have improved the solubility, stability, circulation time, pharmacological effects while reducing toxicity. Among these, nanoparticles (NPs) represent the most widely studied system. Nevertheless, therapeutic efficacy could be further enhanced by combining nanocarriers with a selective targeting strategy, using surface modifications with functional ligands. In this context, galactosyl prodrugs have been explored for targeting senescent cells [24,51–55]. Gal is a galactose-derivate employed for its specific enzymatic targeting mechanism [22,23], as it is preferentially recognized and processed by cells with high β-gal expression. The enzyme cleaves the galactose-nanoparticle bond, allowing the release of the encapsulated active ingredient inside target cells [21].

In this study, liposomes were selected for their biocompatibility, biodegradability, and ability to encapsulate both hydrophilic and lipophilic compounds. The formulation was functionalized with a galactosyl derivative to selectively target senescent cells overexpressing β-Gal, thereby maximizing EA's therapeutic potential through specific delivery.

Gal-LP exhibited a mean particle size of 89.27 ± 0.58 nm, with a narrow size distribution (PdI 0.22 ± 0.00), indicating a homogeneous liposomal population. After EA loading, a slight increase in particle size was observed (110.80 ± 0.17 nm), while maintaining a low polydispersity index (PdI 0.21 ± 0.02), which suggests that drug incorporation did not compromise colloidal uniformity (Table 1). The final EA concentration in the formulation was 0.5 mg/mL. Considering the poor aqueous solubility of EA (9.7 μg/mL), liposomal encapsulation increased its apparent solubility by approximately 51-fold.

The slightly negative Zeta potential values for both formulations (-23.22 ± 1.40 mV for Gal-LP and -24.04 ± 0.04 mV for Gal-LP-EA) indicated good colloidal stability, which was further confirmed by the stability studies.

Table 1
Physical and chemical characterization of Gal-LP and Gal-LP-EA. Data are reported as mean ± SD of n = 4 experiments.

Sample	Size (nm)	PdI	Z-pot (mV)	EE%
Gal-LP	88.76 ± 0.76	0.22 ± 0.00	-23.20 ± 1.39	-
Gal-LP-EA	109.5 ± 0.87	0.21 ± 0.01	-23.94 ± 0.13	80.01 ± 1.33

EE% of 80.44 ± 0.62% demonstrated that Gal-LP-EA effectively incorporated EA within the lipid matrix. This value confirms the suitability of the formulation strategy for drug loading. In this study, a 0.5 mass ratio Gal to the lipid components was selected based on existing literature. Although most studies report ratios of galactose derivative to other components in molar terms [53], utilized it at a 0.5 mass ratio, which is consistent with the approach adopted here.

3.2. Stability study

Physical and chemical Gal-LP-EA profiles were monitored for 30 days at +4 °C, every 5 days, during which vesicle sizes remained constant as did the PdI and Zeta Potential, as shown in Fig. 1. The sizes ranged between 110.8 ± 0.17 nm and 115.2 ± 0.191 nm; PdI fluctuated between 0.21 and 0.23 mV and Zeta Potential changed from -24.04 ± 0.04 at day 0 to -27.33 ± 0.26 mV at day 30.

Chemical stability was monitored concurrently, during which the formulation maintained a consistent profile. The EE% remained stable at approximately 80%, showing only minimal variations throughout the observation period, as illustrated in Fig. 1.

The lipid composition of the bilayer significantly influences the stability of liposomes in human blood serum; higher protein binding typically correlates with greater liposomal instability.

The stability of liposomes in the presence of physiological concentration of HSA was also evaluated, using HSA as a model for biological fluids. DLS analysis confirmed that sizes were not affected, revealing a coexistence of free serum proteins and optimized nanocarrier without any detectable protein corona effect (Table 2) [31]. This is in agreement with that liposomes with a neutral or slightly negative charge containing phosphatidylcholine are highly stable and bind minimal amounts of serum proteins [56].

3.3. In vitro drug release study

The *in vitro* release profile of EA from a methanolic solution (EA-sol) and from Gal-LP-EA was investigated over a 48-h period using the dialysis bag method (Fig. 2). The EA-sol exhibited a rapid and substantial release profile, with approximately 40% of the drug released within the first hour and exceeding 56% within 2 h. Cumulative release further increased to 73% at 6 h, plateauing at ~86–87% at 24 and 48 h, which indicates a fast diffusion of the compound. In contrast, Gal-LP-EA showed a slower and sustained release trend. Approximatively 25% of EA was released within the first hour, with minimal additional release up to 6 h (~28%). Even at 24 h, the cumulative release remained limited (~32%), reaching approximately 40% at 48 h. This sustained-release behavior can be attributed to strong interactions between EA and the liposomal membrane. The lipid composition of the bilayer dictates its fluidity or rigidity, directly influencing the drug diffusion rate. Consequently, Gal-LP-EA successfully reduced the initial burst effect observed for free EA, providing a sustained release profile over 48 h, and preventing rapid and uncontrolled diffusion.

To further characterize the release of EA from liposomes, the flux rate (J) was calculated from the slope of the linear portion of the cumulative release versus time curves divided by the diffusion area of 22 cm^2 [57,58]. The resulting flux values were 0.014 μg/cm^2/h for the liposomal formulation and 0.024 μg/cm^2/h for the methanolic solution. The higher flux observed for the free drug is consistent with its greater

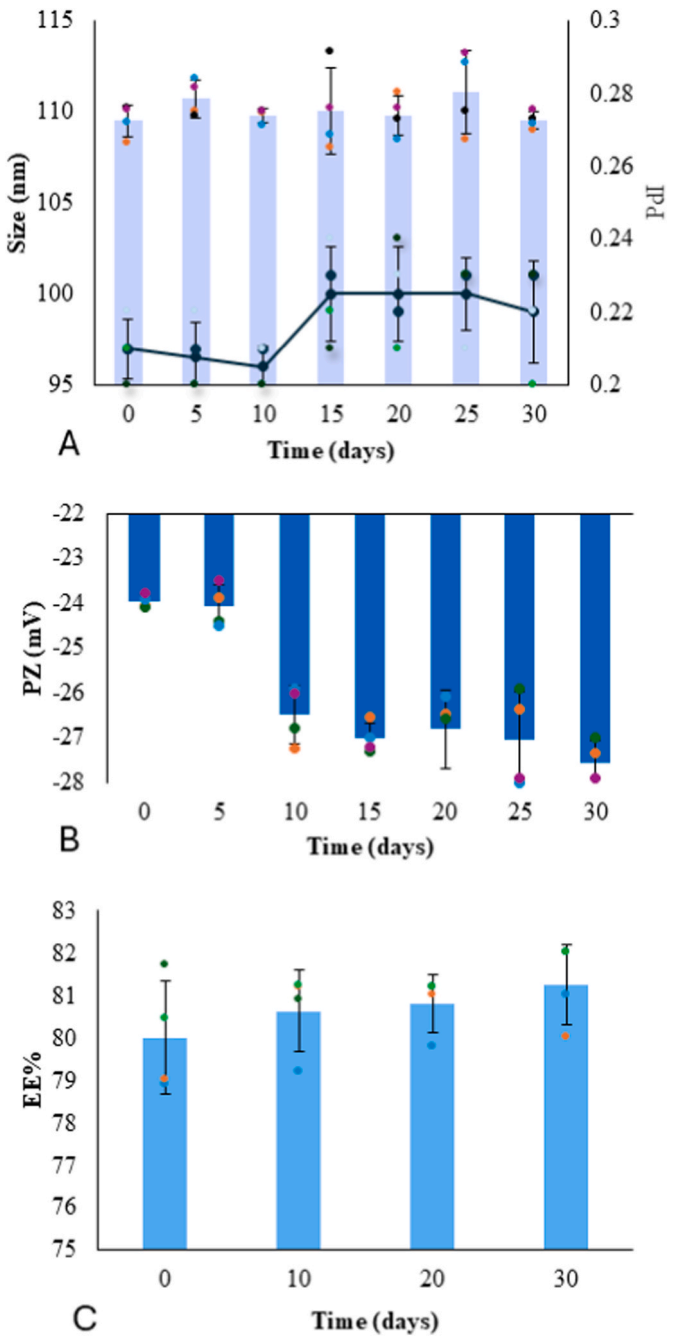

Fig. 1. Storage stability test of Gal-LP-EA at +4 °C for 30 days. Physical stability: (A) Particle size and polydispersity index (PdI); (B) Zeta potential. Chemical stability: Encapsulation Efficiency (C). Data are shown as mean ± SD of n = 4 experiments.

Table 2
Physical stability (Size) of Gal-LP-EA in the presence of HSA. Data are expressed as mean ± SD of n = 3 experiments.

Time (h)	Size (nm) ± SD
0	105.7 ± 0.15
0.5	100.1 ± 0.64
1	101.6 ± 0.78
2	100.5 ± 0.58
3	100.4 ± 0.36

diffusivity in the absence of a carrier system.

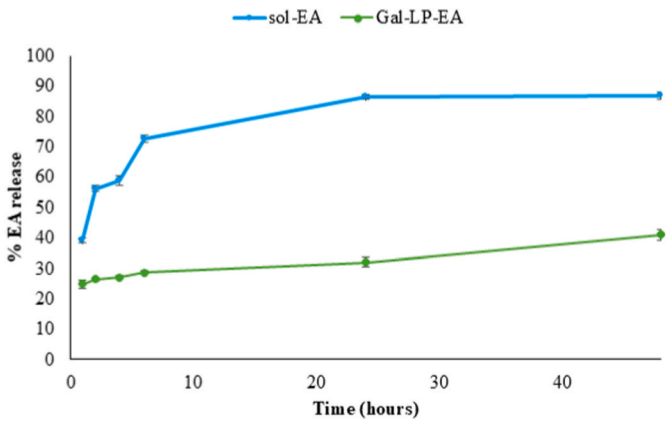

Fig. 2. EA release from EA-sol and Gal-LP-EA. The release medium was withdrawn and analysed after 1, 2, 4, 6, 24 and 48 h for each sample. Data are shown as mean ± SD of n = 4 experiments.

3.4. Parallel Artificial membrane permeability Assay (PAMPA)

The BBB-PAMPA assay was employed to evaluate the passive permeability of EA delivered via the galactosylated liposomal formulation. As expected, free EA exhibited limited permeability, consistent with previous reports describing its poor capacity to diffuse across both the gastrointestinal epithelium and the BBB [18,19,59].

At 4 h, EA in solution displayed a Pe value of 1.72×10^{-6} cm/s, slightly higher than that observed for Gal-LP-EA (1.26×10^{-6} cm/s). A different trend emerged at 8 h, in fact the Pe of free EA decreased to 7.44×10^{-7} cm/s, while Gal-LP-EA maintained a more stable permeability profile with a Pe value of 1.02×10^{-6} cm/s. Although a slight reduction was also observed for the liposomal formulation between 4 and 8 h, the decrease was substantially less pronounced than that of free EA, indicating improved maintenance of permeation over time (Table 3). This behavior indicates that the nanocarrier modulates EA release kinetics, preventing the rapid decline in permeation observed for non-encapsulated compound.

Results were also expressed as the absolute amount of EA permeated through the membrane surface area (μg/cm^2), as shown in Table 4. For the EA-sol, the permeated amount increased from 1.04 ± 0.02 μg/cm^2 at 4 h to 2.12 ± 0.15 μg/cm^2 at 8 h, indicating a time-dependent accumulation of the compound in the acceptor compartment. Notably, the galactosylated liposomes exhibited higher permeation at both time points, reaching 5.84 ± 0.60 μg/cm^2 at 4 h and 10.07 ± 1.12 μg/cm^2 at 8 h, corresponding to an approximately 5.6-fold and 4.7-fold increase over free EA at 4 and 8 h, respectively.

Recovery values remained above 80% at 4 and 8 h, confirming the robustness and reliability of the experiment. Importantly, the permeability coefficients obtained (10^{-6} cm/s range) are consistent with values typically reported for BBB-PAMPA assays in the literature [19], supporting the methodological validity of the study. Overall, these findings demonstrate that liposomes offer an important contribution in increasing the passive permeation of EA, supporting their potential use as delivery systems for improving the bioavailability of poorly permeable compounds.

Table 3
Pe values (cm/s) referred to EA solution in MeOH (0.3 mg/mL) diluted with PBS: EtOH (80:20) to 0.1 mg/mL and to Gal-LP-EA. Data are expressed as mean ± SD of n = 4 experiments.

Time	Pe (cm/s)			
	EA-sol	SD	Gal-LP-EA	SD
4h	1.72E-06	2.95E-07	1.19E-06	1.51E-07
8h	7.44E-07	3.18E-08	1.02E-06	5.94E-08

Table 4
Absorbed dose (A) of EA from Gal-LP-EA and from EA-sol after 4 h and 8h of incubation. Data are expressed as mean ± SD of n = 4 experiments.

	A μg/cm^2	
EA-sol	1.04 ± 0.02 (A_4)	2.12 ± 0.15 (A_8)
Gal-LP-EA	5.53 ± 0.77 (A_4)	10.03 ± 0.65 (A_8)

While PAMPA allows only for the evaluation of passive mechanisms, the results proved a significant increase in the Pe value, the total amount of EA permeated, and the absorbed dose due to the liposomal formulation. Although it is a simplified assay, it is highly useful in pre-formulation studies for an initial evaluation of the permeability of single substances. The PAMPA assay provides preliminary and useful indications regarding the carrier, but further cellular and *in vivo* studies are required to confirm its potential use as a delivery system for enhancing BBB bioavailability.

3.5. Cellular study

EA has demonstrated many therapeutic benefits as confirmed by *in vitro* [60,61], *in vivo* [62,63] and clinical studies [64]. Rahimi and colleagues demonstrated that EA (0.01-10 μM) exhibited anti-aging properties against damage caused by D-galactose in human neuroblastoma cell line SH-SY5Y [65]. Another study showed that EA (0.5, 1, 5, and 10 μM) reduced NO generation and TNF-α levels in BV2 microglial cells stimulated by LPS [66]. In 2015, Alfredsson and colleagues showed that EA (50 μM) decreased cell detachment, loss of viability, and activation of apoptosis in neuroblastoma cells (SH-SY5Y) undergoing differentiation with ATRA and TPA [67]. Furthermore, EA 30 μM decreased ROS production and astrocyte cell death in rat primary astrocytes treated with cadmium [68]. Rizk et al. [69] demonstrated that co-administration of EA (10 mg/kg) along with doxorubicin suppressed brain contents of lipid peroxides, reduced TNF-α and caspase-3 concentrations, and improved the GSH concentration in rats treated for 14 days.

In this study EA and Gal-LP-EA were tested in an *in vitro* model of senescence. It's already demonstrated that the exposure to the anticancer drug doxorubicin can be able to induce senescence in fibroblasts [70] but also in primary rat astrocytes cultures [37]. To investigate the ability of doxorubicin to induce senescence in glial cells, we cultured mixed rat primary glial cells obtained by cerebral cortex of 2 post-natal day rat pups. The cells were then treated with 250 nM of doxorubicin for 24 h. Therefore, the influence of the liposomal formulation in increasing the EA delivery and its activity at the cerebral level to counteract the effect of doxorubicin was evaluated.

3.5.1. Effects of EA and gal-LP-EA on mixed glial cells

To evaluate the safety and tolerability of EA and Gal-LP-EA, glial cells were exposed 24 h to EA and Gal-LP-EA (5 -25 μg/mL) and sister cultures were exposed to 250 nM of doxorubicin for 24 h in the presence or absence of EA or Gal-LP-EA (5-10 μg/mL). The cytotoxicity of EA and Gal-LP-EA alone and in combination with doxorubicin were assessed with LDH assays, as indicator of cell death and cytotoxicity, with Triton-X 0.01% used as the positive control. Fig. 3A shows that when present in the incubation medium, EA or Gal-LP-EA did not induce significant differences in LDH levels compared to the control. Similarly, 24 h of doxorubicin treatment did not alter the LDH dosages when present in the incubation medium alone or alongside EA or Gal-LP-EA, compared to the control (CRL) cells (Fig. 3C). Moreover, to better evaluate long-term

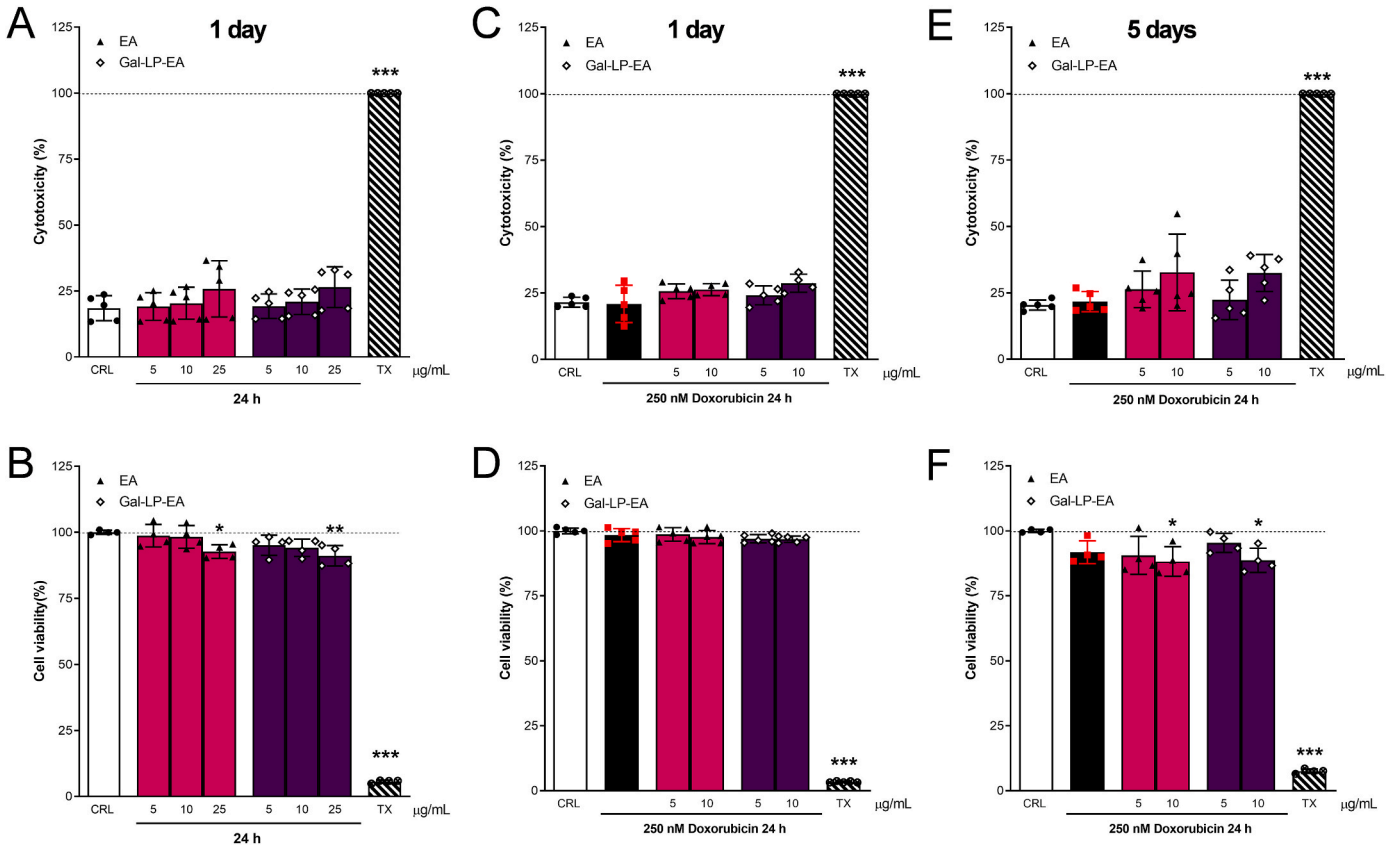

Fig. 3. Rat mixed glial cells cytotoxicity and cell viability by LDH and MTT assays. Glial cells were exposed for 24 h to EA or Gal-LP-EA (5-25 μg/mL) (A-B) or to 250 nM doxorubicin alone or in presence of EA and Gal-LP-EA and LDH and MTT assays were performed 24 h (C-D) or 4 days (E-F) after the end of treatments. Data are expressed as a percentage of Triton X-100 (TX) and CRL, which represent, respectively, the maximum cell cytotoxicity and cell viability. Values represent the mean ± SD of at least four experiments performed in duplicate. *p < 0.05, **p < 0.01 and ***p < 0.001 vs. CRL (one-way ANOVA followed by Dunnett's test).

safety and tolerability following 24 h of treatment with EA and Gal-LP-EA in the presence of 250 nM of doxorubicin, we cultured glial cells for an additional 4 days after a medium change, performing the LDH assay on the 5th day of culture. As shown in Fig. 3E, after 5 days of culture, doxorubicin alone or in the presence of EA and EA-loaded liposomes did not induce significant cytotoxicity compared to the control. In cell viability assays performed using the MTT method, significant differences were observed between cells treated with EA ($p = 0.0226$ vs CRL) and Gal-LP-EA ($p = 0.0045$ vs CRL) at the concentration of 25 μg/mL relative to CRL cells (Fig. 3B), for this reason in the subsequent experiments we selected the dose of 5 and 10 μg/mL of EA and liposomes. Furthermore, we observed significant differences between cells treated with doxorubicin plus EA ($p = 0.0189$ vs CRL) and Gal-LP-EA ($p = 0.0260$ vs CRL) at the concentration of 10 μg/mL relative to CRL cells at 5 days (Fig. 3F).

3.5.2. *EA and gal-LP-EA are able to reduce the senescent phenotype induced by doxorubicin acting on SIRT1/p53/p21 pathway in mixed glial cells*

To evaluate the ability of doxorubicin to induce senescence and the capacity of EA and Gal-LP-EA to counteract the doxorubicin-induced senescent phenotype, this study utilized glial cells exposed to doxorubicin for 24 h as an *in vitro* model. Doxorubicin, a chemotherapeutic agent widely used in cancer treatment, is able to intercalate into DNA strands, inhibit DNA and RNA synthesis, and generate reactive oxygen species (ROS) leading to significant DNA damage. Consequently, it induces the upregulation of cell cycle inhibitors such as p21, a key player in halting cell proliferation and triggering the cellular senescence [37,71,72]. Based on these considerations, we analysed the effects of EA and Gal-LP-EA in glial cells exposed to 250 nM doxorubicin for 24 h by RT-qPCR. Evidence of doxorubicin-induced senescence has been widely reported in the literature. For instance, Marques and colleagues reported that 72 h of exposure to 250 nM doxorubicin was able to induce senescence in primary rat astrocytes by acting on several key markers, as confirmed by the elevated β-galactosidase activity, decreased lamin B1 staining and expression, as well as increased p21 levels and expression [37]. Similarly, the senescent phenotype was induced in human-derived primary skin fibroblast cells (using 250 nM doxorubicin for 24 h) [9], in the hepatocellular carcinoma cell line HuH-7 (100 nM for 48 h) [7], and in both the HL-1 cardiac muscle cell line and human AC16 cardiomyoblasts (100 nM for 24 h) [5].

Fig. 4 shows that, in mixed glial cells, 250 nM doxorubicin for 24 induced a significant increase in mRNA expression levels of the senescence markers p53 (Fig. 4A; $p = 0.0213$ vs CRL) and p21 (Fig. 4B; $p = 0.0001$ vs CRL) and a decrease of SIRT1 (Fig. 4C), compared to control. When present in the incubation medium EA was partially able to revert the increased mRNA expression levels of p53 ($p = 0.6711$ and $p = 0.6137$ vs doxorubicin) and p21 ($p = 0.5698$ and $p = 0.0803$ vs doxorubicin) and the decreased mRNA levels of SIRT1 induced by 24 h of 250 nM of doxorubicin. Moreover, Gal-LP-EA was able to induce a significant decrease of the doxorubicin-increased mRNA expression levels of p53 (at 10 μg/mL; $p = 0.0398$ vs doxorubicin) and p21 (at both doses tested; $p = 0.0179$ and $p = 0.0071$ vs doxorubicin) and was partially able to increase the decreased SIRT1($p > 0.9999$ and $p = 0.9982$ vs doxorubicin) mRNA levels induced by doxorubicin.

3.5.3. *Effects of EA and gal-LP-EA on the DNA damage response and the reduced proliferation induced by doxorubicin in mixed cortical glial cells*

Cellular senescence is characterized by stable cell cycle arrest, nuclear enlargement, decreased proliferation, and the acquisition of distinct morphological and molecular features in various cell types, including primary rat and human astrocytes [37,73].

To assess the senescent phenotype in mixed cortical glial cells induced by doxorubicin and the possible effects of EA and Gal-LP-EA, we also used western blotting to investigate the expression of γ-H2AX, as a marker of double-strand DNA breaks [74] and the expression of Ki67 as a marker of cellular proliferation, which is progressively expressed during the S phase of the cell cycle (replication phase) [75] in our *in vitro* model of senescence. Based on the RT-qPCR results, we selected the concentration of 10 μg/mL of EA and Gal-LP-EA as better to evaluate their effects on protein expression. As shown on Figs. 2 and 54 h of 250 nM doxorubicin induced a significant reduction of Ki67 (Fig. 5A and B; $p = 0.0009$ vs CRL) and a significant increase of the expression of γ-H2AX (Fig. 5C and D; $p < 0.0001$ vs CRL). As reported in the literature, senescent cells are characterized by accumulation of DNA damage and cycle arrest [74,76–78]. When present in the incubation medium EA ($p = 0.4036$ vs doxorubicin) and Gal-LP-EA ($p = 0.0574$ vs doxorubicin) were able to increase the decreased levels of Ki67 induced by

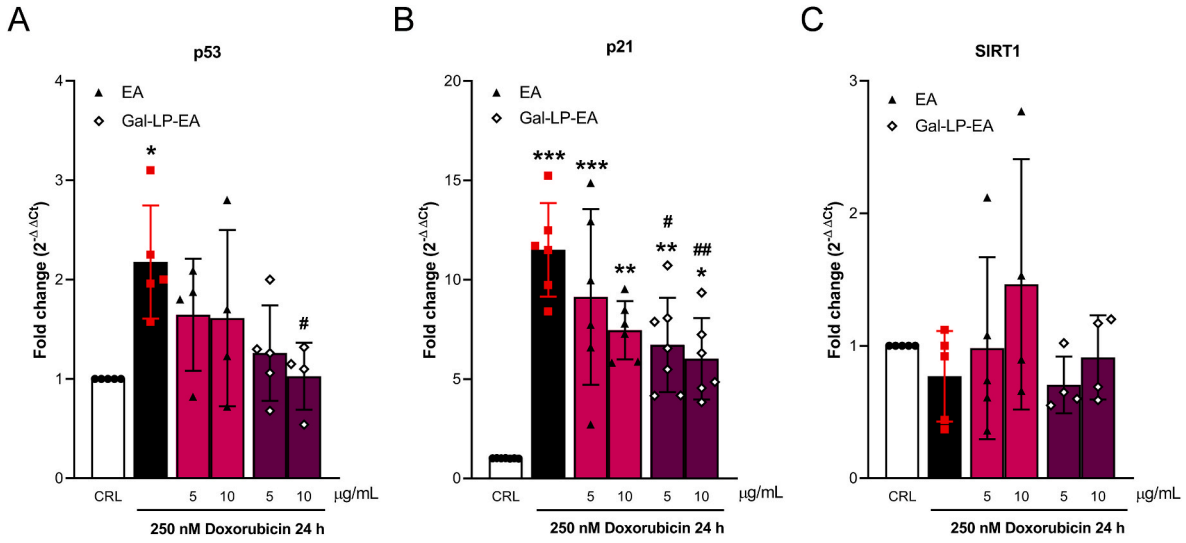

Fig. 4. The mRNA levels of p53, p21 and SIRT1 in mixed glial cells exposed to doxorubicin alone or in the presence of EA and Gal-LP-EA. EA was partially able to revert the increase in mRNA expression levels of p53 (A) and p21 (B) and the decreased mRNA levels of SIRT1 (C) induced by doxorubicin. Gal-LP-EA induced a significant decrease of the doxorubicin-increased mRNA levels of p53 (A) and p21 (B) and partially increased the decreased SIRT1 (C) mRNA levels induced by doxorubicin. Bars represent the mean ± SD from at least four independent experiments from different glia cells preparations and each dot is the pool of two wells. *p < 0.05, **p < 0.01 and ***p < 0.001 vs. CRL; #p < 0.05 and ##p < 0.01 vs doxorubicin (ANOVA + Tukey's w test).

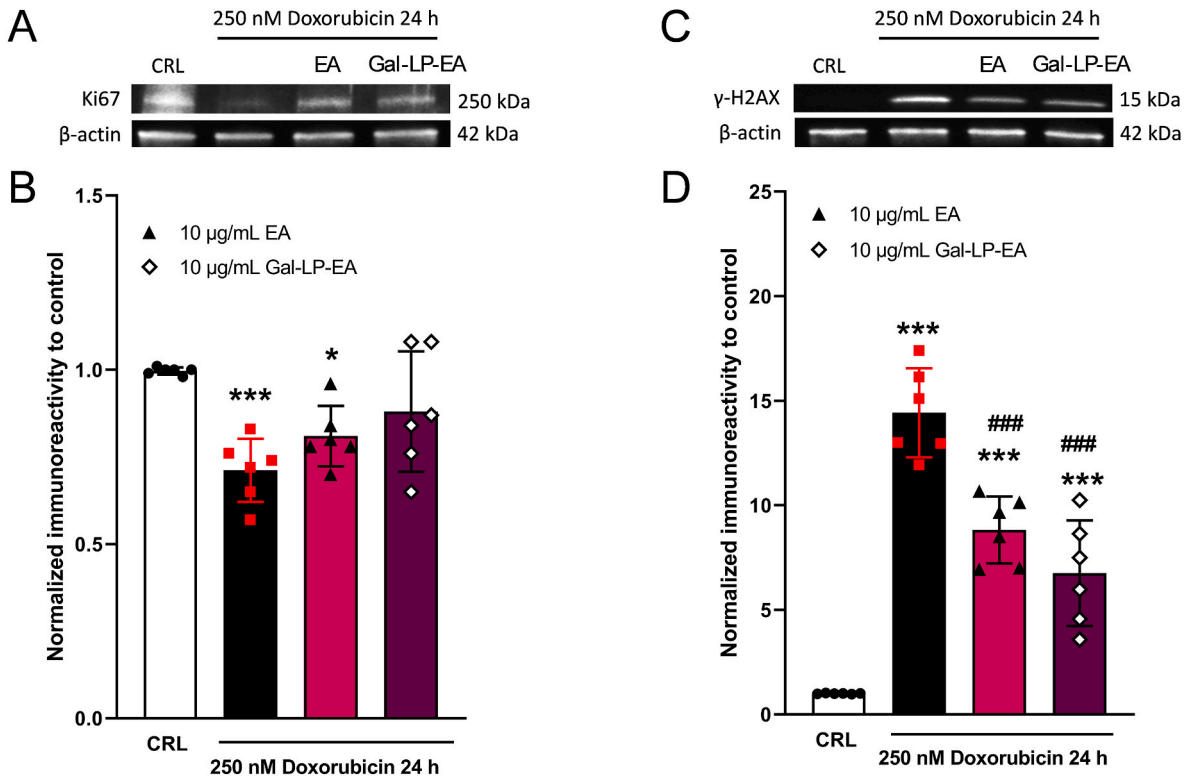

Fig. 5. The effects of EA and Gal-LP-EA on senescence markers in mixed glial cells exposed to doxorubicin. Cells were exposed to 250 nM doxorubicin for 24 h and then processed for WB. The compounds were present in the incubation medium during doxorubicin exposure. Representative blots for Ki67 (A) and γ-H2AX (C) or β-actin. (A, C) The quantitative analysis of immunoreactive bands showing that EA and Gal-LP-EA were partially able to revert the decreased levels of Ki67 induced by doxorubicin (B). Moreover, EA and Gal-LP-EA induced a significant decrease of the increased levels of γ-H2AX induced by doxorubicin (D). Bars represent the mean ± SD from six independent experiments from different glia cell preparations, and each dot is the pool of two wells. *p < 0.05 and ***p < 0.001 vs. CRL; ###p < 0.001 vs doxorubicin (ANOVA + Tukey's w test).

doxorubicin (Fig. 5A and B). Moreover, EA (p = 0.0002 vs doxorubicin) and Gal-LP-EA (p < 0.0001 vs doxorubicin) significantly reverted the increased levels of γ-H2AX induced by doxorubicin. This effect is more significant for the Gal-LP-EA compared to EA (Fig. 5C and D). In this study we observed marker changes (p53, p21, SIRT1, γ-H2AX) without demonstrating causal pathways, but in the literature is well reported that SIRT1 down-regulation, p53 hyperacetylation/activation, p21 induction, and γ-H2AX accumulation as a canonical driver of cellular senescence and DNA damage responses [79].

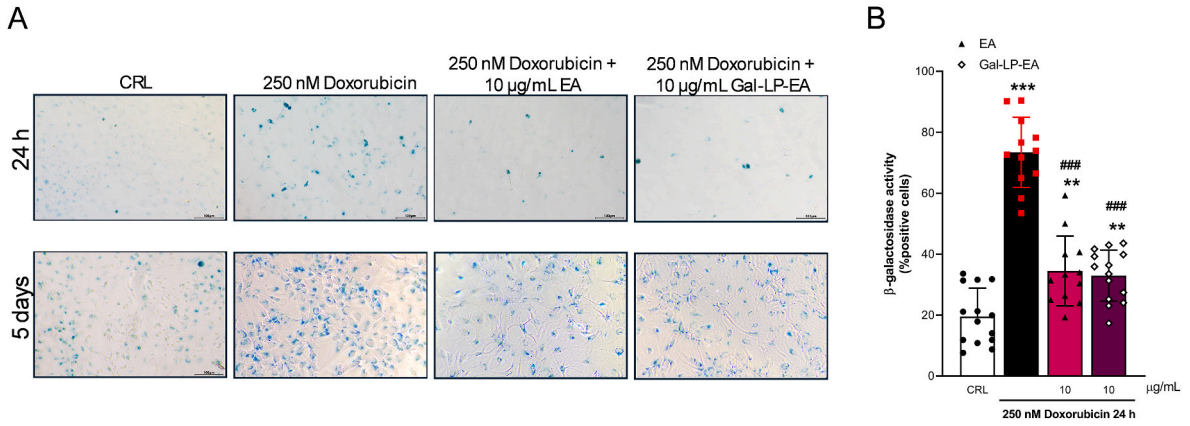

Fig. 6. Effects of EA and Gal-LP-EA on the SA-β-gal induced by 24 h doxorubicin in mixed glial cells. (A) Representative bright-field images of SA-β-gal staining in mixed glial cultures exposed to 250 nM doxorubicin for 24 h in the absence or presence of EA or Gal-LP-EA. SA-β-gal activity was evaluated immediately after treatment (24 h) and four days after doxorubicin exposure (five days). The SA-β-gal staining showed increased enzymatic activity in doxorubicin-treated glial cells compared to control. EA and Gal-LP-EA were able to reduce the increased SA-β-gal activity induced by 24 h doxorubicin exposure. Scale bar = 100 μm. (B) Quantification of SA-β-gal-positive cells evaluated four days after doxorubicin exposure (five days) and expressed as the percentage of positive cells relative to the total number of cells. Doxorubicin significantly increased cellular senescence compared with control cultures, whereas EA and Gal-LP-EA significantly reduced the proportion of SA-β-gal-positive cells. Bars represent the mean ± SD of at least twelve field per condition from four independent experiments from different glial cells preparations. Statistical analysis was performed using one-way ANOVA followed by Tukey's multiple-comparisons test. * *p < 0.01 and ***p < 0.001 vs. CRL; ####p < 0.0001 vs doxorubicin.

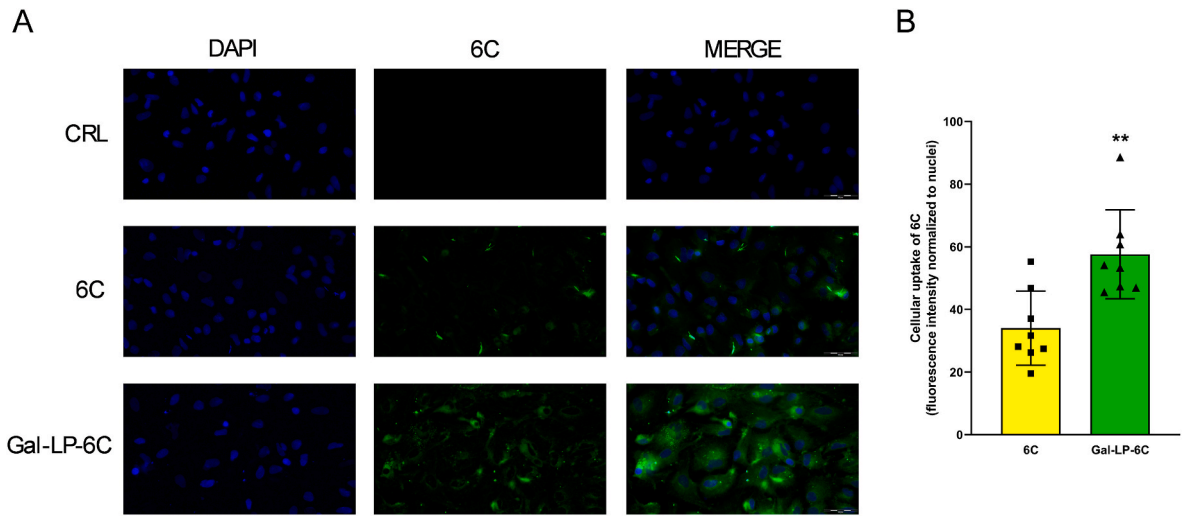

Fig. 7. Cellular uptake of 6C and Gal-LP-6C by mixed glial cells after 1 h incubation at 37 °C. (A) Qualitative images of nuclei stained with DAPI (blue), 6-C (green) and their merge. Scale bar: 50 μm. (B) Quantitative analysis of cellular uptake showed that the formulation Gal-LP-6C increased significantly the fluorescence intensity compared to free 6C. Fluorescence intensity of 6C (Ex/Em: 485/524) was normalized to cell number. Bars represent the mean ± SD of eight field per condition from four independent experiments from different glial cells preparations. **$p < 0.01$ vs 6C (Student's t-test). (For interpretation of the references to colour in this figure legend, the reader is referred to the Web version of this article.)

3.5.4. EA and gal-LP-EA reduce the elevated SA-β-gal levels induced by doxorubicin exposure in mixed glial cells

It is well established in the literature that senescence is a state of stable growth arrest accompanied by a hypersecretory and proinflammatory phenotype, recognized as the senescence-associated secretory phenotype (SASP) [77]. This stasis in cell cycle progression is accompanied by discernible shifts in cellular morphology and architecture, along with key cellular and molecular changes, including increased β-galactosidase activity, commonly used as a senescence-associated marker (SA-β-gal) [78]. Indeed, as reported in Marques and colleagues, immortalized rat microglial CHME-5 cells exposed to doxorubicin for 48 h showed an increase staining of the senescence-associated β-galactosidase SA-β-gal [36]. In the present study, SA-β-gal activity and the potential protective effects of EA and Gal-LP-EA were assessed in our *in vitro* model of mixed cortical glial cells using a Senescence β-Galactosidase Staining Kit. Furthermore, SA-β-gal activity was evaluated 5 days post-exposure to doxorubicin (24 h), both alone and in combination with EA or Gal-LP-EA.

Representative images of SA-β-gal staining are shown in Fig. 6A. Exposure of mixed cortical glial cultures to doxorubicin markedly increased the number of SA-β-gal-positive cells compared with untreated controls, both immediately after treatment (24 h) and four days after exposure, indicating the induction and persistence of a senescent phenotype. Furthermore, when present in the incubation medium, EA or Gal-LP-EA reduced the abundance of SA-β-gal-positive cells, as evidenced by the lower intensity and frequency of blue staining.

Quantitative analysis confirmed these observations (Fig. 6B). Doxorubicin significantly increased the percentage of SA-β-gal-positive cells compared with control cultures. Both EA and Gal-LP-EA significantly attenuated the doxorubicin-induced increase in SA-β-gal activity.

The present findings provide further evidence that EA and Gal-LP-EA mitigate doxorubicin-induced cellular senescence in mixed glial cultures. Doxorubicin exposure induced a marked increase in SA-β-gal activity, consistent with previous reports describing the ability of anthracyclines to trigger a senescence-like phenotype in glial cells. Importantly, both EA and Gal-LP-EA significantly reduced the proportion of SA-β-gal-positive cells, indicating attenuation of the senescent phenotype.

3.5.5. Cellular uptake

The Gal-LP-6C formulation used for uptake studies was first characterized physico-chemically, exhibiting a mean diameter of 165.8 ± 0.09 nm, a PDI of 0.43 ± 0.02, a surface charge of −7.85 ± 0.06 mV, and a high encapsulation efficiency (98.23 ± 1.69%). Cellular uptake studies were then performed to evaluate if the formulation enhanced EA permeation into glial cells. Mixed glial cells were exposed for 1 h to either Gal-LP-6C loaded with 0.2 mg/mL of 6C (diluted 1:40 in culture medium) or a saturated solution of free 6C. Nuclei were counterstained blue with DAPI. Fig. 7 displays both qualitative fluorescence microscopy images and the corresponding quantitative analysis of fluorescence intensity after 1 h of incubation. While both free 6C and the liposomes successfully penetrated the cells, glial cells treated with Gal-LP-6C exhibited significantly higher fluorescence intensity than those treated with free 6C ($p = 0.0028$ vs 6C). Notably, the liposomal formulation induced an approximately 2-fold increase in fluorescence intensity compared to the free probe.

4. Conclusions

Galactose-modified liposomes have been optimized for the delivery of EA and to improve its therapeutic efficacy in counteracting doxorubicin-induced senescence in mixed primary glial cells.

The strategy leverages the overexpression of the enzyme β-galactosidase (β-gal) in senescent cells, utilizing liposomes functionalized with galactosylceramide to ensure selective recognition and processing by target cells.

In vitro characterization demonstrated that this nanocarrier enhanced the aqueous solubility of EA, exhibited excellent stability, and achieved a sustained release profile. Furthermore, Gal-LP-EA improved the permeability of EA in the BBB-PAMPA assay.

Using a preclinical *in vitro* model of chemotherapy-induced senescence both EA and Gal-LP-EA demonstrated the capacity to counteract the senescent phenotype. Specifically, Gal-LP-EA counteracted the doxorubicin-induced downregulation of Ki67, significantly attenuated γ-H2AX levels, and reduced SA-β-gal activity. Despite all the limitations of the *in vitro* model of mixed glial cells, the results of this multidisciplinary study highlight the potential of Gal-coated liposomes as novel delivery strategy for mitigating senescence processes. Integrating EA's pharmacological potential with galactosyl-functionalized nanocarriers could represent a promising approach for the selective clearance of senescent cells in the age-related diseases.

Funding

This research was funded by Fondi di Ateneo 2025 to Elisa Landucci and Maria Camilla Bergonzi.

CRediT authorship contribution statement

Elisa Landucci: Conceptualization, Funding acquisition, Writing – original draft, Writing – review & editing. **Rebecca Castellacci:** Formal analysis, Investigation, Writing – original draft. **Alba Puente-Sanz:** Formal analysis, Investigation, Writing – original draft. **Costanza Mazzantini:** Formal analysis, Investigation, Writing – original draft. **Domenico E. Pellegrini-Giampietro:** Writing – review & editing. **Anna Rita Bilia:** Writing – review & editing. **Maria Camilla Bergonzi:** Conceptualization, Funding acquisition, Writing – original draft, Writing – review & editing.

Declaration of competing interest

The authors declare that they have no known competing financial interests or personal relationships that could have appeared to influence the work reported in this paper.

Data availability

Data will be made available on request.

References

[1] T. Saliev, P.B. Singh, Targeting senescence: a review of senolytics and senomorphics in anti-aging interventions, Biomolecules 15 (2025) 860, https://doi.org/10.3390/biom15060860.
[2] G. Carreno, R. Guiho, J.P. Martinez-Barbera, Cell senescence in neuropathology: a focus on neurodegeneration and tumours, Neuropathol, Appl. Neurobiol. 47 (2021) 359–378, https://doi.org/10.1111/nan.12689.
[3] D. McHugh, I. Durán, J. Gil, Senescence as a therapeutic target in cancer and age-related diseases, Nat. Rev. Drug Discov. 24 (2025) 57–71, https://doi.org/10.1038/s41573-024-01074-4.
[4] X. Li, X. Yan, Q. Chen, S. Mai, G1/S arrest: a key mechanism of cellular aging and replicative senescence, Biogerontology 27 (2026) 40, https://doi.org/10.1007/s10522-025-10378-w.
[5] W. Fan, J. Huang, Z. Guo, A. Zhong, X. Tong, X. Li, W. Li, Y. Chen, Y. Chen, X. Lin, J. Xu, D. Huang, Y. Zhang, B. Wang, Melatonin suppresses cellular senescence in diabetic kidney disease though the Wnt/β-catenin signaling pathway, Eur. J. Pharmacol. 1015 (2026) 178541, https://doi.org/10.1016/j.ejphar.2026.178541.
[6] T. Xu, X. Wu, Y. Zhang, Y. Cai, X. Zhang, Q. Zeng, J. Luo, J. Wei, T. Chen, L-Tryptophan produced by Bifidobacterium pseudocatenulatum NCU-08 delays aging in SAMP8 mice by activating the Sirt1/P53/P21/Rb signaling pathway, Aging Cell 24 (2025) e70166, https://doi.org/10.1111/acel.70166.
[7] M. Karabicici, S. Alptekin, Z. Fırtına Karagonlar, E. Erdal, Doxorubicin-induced senescence promotes stemness and tumorigenicity in EpCAM-/CD133- nonstem cell population in hepatocellular carcinoma cell line, HuH-7, Mol. Oncol. 15 (2021) 2185–2202, https://doi.org/10.1002/1878-0261.12916.
[8] H. Abdeahad, D.G. Moreno, S.I. Bloom, L. Norman, L.A. Lesniewski, A.J. Donato, MitoQ reduces senescence burden in doxorubicin-treated endothelial cells by reducing mitochondrial ROS and DNA damage, Am. J. Physiol. Heart Circ. Physiol. 329 (2025) H1154–H1161, https://doi.org/10.1152/ajpheart.00568.2025.
[9] I. Heckenbach, G.V. Mkrtchyan, M. Ben Ezra, D. Bakula, J.S. Madsen, M.H. Nielsen, D. Oró, B. Osborne, A.J. Covarrubias, M.L. Idda, M. Gorospe, L. Mortensen, E. Verdin, R. Westendorp, M. Scheibye-Knudsen, Nuclear morphology is a deep learning biomarker of cellular senescence, Nat. Aging 2 (2022) 742–755, https://doi.org/10.1038/s43587-022-00263-3.
[10] Y.-F. Chen, R.-Q. Qi, L. Zhao, L.-R. Liang, J.-W. Song, X.-Y. Zhou, Y.-H. Chen, S.-Y. Wang, Q. Wang, Y. Liu, Y. Dong, X.-Y. Liu, J. Li, J.-C. Zhong, Aprocitentan mitigates doxorubicin-induced cardiotoxicity by inhibiting cuproptosis, oxidative stress, and mitochondrial impairments via the activation of sirtuin 7, Int. Immunopharmacol. 148 (2025) 114141, https://doi.org/10.1016/j.intimp.2025.114141.
[11] K. Macova, D. Mjartinova, L. Fialova, D. Nakladal, D. Fricova, Senescence in neural cell lines: comparative insights from SH-SY5Y and ReNcell VM, Gen. Physiol. Biophys. 44 (2025) 39–49, https://doi.org/10.4149/gpb_2024028.
[12] F. Alshaebi, A. Sciortino, R. Kayed, The role of glial cell senescence in alzheimer's disease, J. Neurochem. 169 (2025) e70051, https://doi.org/10.1111/jnc.70051.
[13] L. de S. Hayashide, B. Pessoa, G. Dias, B. Pontes, R.S. Pinto, L.P. Diniz, From neuron-centric to glia-centric: how aging glial networks drive neurodegenerative disease, J. Neurochem. 170 (2026) e70361, https://doi.org/10.1111/jnc.70361.
[14] J.M. Van Deursen, The role of senescent cells in ageing, Nature 509 (2014) 439–446, https://doi.org/10.1038/nature13193.
[15] A. Gupta, A.K. Singh, R. Kumar, S. Jamieson, A.K. Pandey, A. Bishayee, Neuroprotective potential of ellagic acid: a critical review, Adv. Nutr. 12 (2021) 1211–1238, https://doi.org/10.1093/advances/nmab007.
[16] D. Sacks, B. Baxter, B.C.V. Campbell, J.S. Carpenter, C. Cognard, D. Dippel, M. Eesa, U. Fischer, K. Hausegger, J.A. Hirsch, M. Shazam Hussain, O. Jansen, M. V. Jayaraman, A.A. Khalessi, B.W. Kluck, S. Lavine, P.M. Meyers, S. Ramee, D. A. Rüfenacht, C.M. Schirmer, D. Vorwerk, Multisociety consensus quality improvement revised consensus statement for endovascular therapy of acute ischemic stroke, Int. J. Stroke 13 (2018) 612–632, https://doi.org/10.1177/1747493018778713.
[17] N. Naghibi, A. Sadeghi, S. Movahedinia, M. Rahimi Naiini, M.A. Rajizadeh, F. Bahri, M. Nazari-Robati, Ellagic acid ameliorates aging-induced renal oxidative damage through upregulating SIRT1 and NRF2, BMC Complement. Med. Ther. 23 (2023) 77, https://doi.org/10.1186/s12906-023-03907-y.
[18] I. Nyamba, A. Lechanteur, R. Semdé, B. Evrard, Physical formulation approaches for improving aqueous solubility and bioavailability of ellagic acid: a review, Eur. J. Pharm. Biopharm. 159 (2021) 198–210, https://doi.org/10.1016/j.ejpb.2020.11.004.
[19] R. Osztie, T. Czeglédi, S. Ross, B. Stipsicz, E. Kalydi, S. Béni, I. Boldizsár, E. Riethmüller, S.E. Bősze, Á. Alberti, Comprehensive characterization of phytochemical composition, membrane permeability, and antiproliferative activity of Juglans nigra polyphenols, Int. J. Mol. Sci. 25 (2024) 6930, https://doi.org/10.3390/ijms25136930.
[20] M.A. Khan, A. Khan, M. Azam, K.S. Allemailem, F. Alrumaihi, A. Almatroudi, F. A. Alhumaydhi, F. Azam, S.H. Khan, S.F.F. Zofair, S. Ahmad, H. Younus, Liposomal ellagic acid alleviates cyclophosphamide-induced toxicity and eliminates the systemic Cryptococcus neoformans infection in leukopenic mice, Pharmaceutics 13 (2021) 882, https://doi.org/10.3390/pharmaceutics13060882.
[21] C. Battisegola, C. Billi, M.C. Molaro, M.E. Schiano, M. Nieddu, M. Failla, E. Marini, S. Albrizio, F. Sodano, M.G. Rimoli, Galactose: a versatile vector unveiling the potentials in drug delivery, diagnostics, and theranostics, Pharm. Times 17 (2024) 308, https://doi.org/10.3390/ph17030308. Page 308 17 (2024).
[22] A. Saraswat, H.P. Vemana, V.V. Dukhande, K. Patel, Galactose-decorated liver tumor-specific nanoliposomes incorporating selective BRD4-targeted PROTAC for hepatocellular carcinoma therapy, Heliyon 8 (2022) e08702, https://doi.org/10.1016/j.heliyon.2021.e08702.
[23] H.R. Oh, H.Y. Jo, J.S. Park, D.E. Kim, J.Y. Cho, P.H. Kim, K.S. Kim, Galactosylated liposomes for targeted Co-Delivery of doxorubicin/vimentin siRNA to hepatocellular carcinoma, Nanomaterials 6 (2016) 141, https://doi.org/10.3390/nano6080141, 6 (2016) 141.
[24] D. Muñoz-Espín, M. Rovira, I. Galiana, C. Giménez, B. Lozano-Torres, M. Paez-Ribes, S. Llanos, S. Chaib, M. Muñoz-Martín, A.C. Ucero, G. Garaulet, F. Mulero, S. G. Dann, T. VanArsdale, D.J. Shields, A. Bernardos, J.R. Murguía, R. Martínez-Máñez, M. Serrano, A versatile drug delivery system targeting senescent cells, EMBO Mol. Med. 10 (2018), https://doi.org/10.15252/emmm.201809355.
[25] X. Wei, D. Yang, Z. Xing, C. Zhao, L. Wang, Y. Fan, H. Nie, H. Liu, Quercetin loaded liposomes modified with galactosylated chitosan prevent LPS/D-GalN induced acute liver injury, Mater. Sci. Eng., C 131 (2021) 112527, https://doi.org/10.1016/j.msec.2021.112527.
[26] E. Landucci, C. Mazzantini, M. Calvani, D.E. Pellegrini-Giampietro, M.C. Bergonzi, Evaluation of conventional and hyaluronic acid-coated thymoquinone liposomes in an in vitro model of dry eye, Pharmaceutics 15 (2023) 578, https://doi.org/10.3390/pharmaceutics15020578.
[27] G. Zuccari, S. Baldassari, G. Ailuno, F. Turrini, S. Alfei, G. Caviglioli, Formulation strategies to improve oral bioavailability of ellagic acid, Appl. Sci. 10 (2020) 3353, https://doi.org/10.3390/APP10103353, 10 (2020) 3353.
[28] I. Bala, V. Bhardwaj, S. Hariharan, M.N.V.R. Kumar, Analytical methods for assay of ellagic acid and its solubility studies, J. Pharm. Biomed. Anal. 40 (2006) 206–210, https://doi.org/10.1016/j.jpba.2005.07.006.
[29] M. Vasarri, L. Ponti, D. Degl'Innocenti, M.C. Bergonzi, Usnic acid-loaded polymeric micelles: an optimal Migrastatic-Acting formulation in human SH-SY5Y neuroblastoma cells, Pharmaceuticals 15 (2022) 1207, https://doi.org/10.3390/ph15101207.
[30] M.C. Bergonzi, M. Vasarri, G. Marroncini, E. Barletta, D. Degl'Innocenti, Thymoquinone-loaded Soluplus®-Solutol® HS15 mixed micelles: preparation, in vitro characterization, and effect on the SH-SY5Y cell migration, Molecules 25 (2020) 4707, https://doi.org/10.3390/molecules25204707.
[31] G. Graverini, V. Piazzini, E. Landucci, D. Pantano, P. Nardiello, F. Casamenti, D. E. Pellegrini-Giampietro, A.R. Bilia, M.C. Bergonzi, Solid lipid nanoparticles for delivery of andrographolide across the blood-brain barrier: in vitro and in vivo evaluation, Colloids Surf. B Biointerfaces 161 (2018) 302–313, https://doi.org/10.1016/j.colsurfb.2017.10.062.
[32] V. Piazzini, E. Landucci, M. Urru, A. Chiarugi, D.E. Pellegrini-Giampietro, A. R. Bilia, M.C. Bergonzi, Enhanced dissolution, permeation and oral bioavailability of aripiprazole mixed micelles: in vitro and in vivo evaluation, Int. J. Pharm. 583 (2020) 119361, https://doi.org/10.1016/j.ijpharm.2020.119361.
[33] V. Piazzini, E. Landucci, G. Graverini, D.E. Pellegrini-Giampietro, A.R. Bilia, M. C. Bergonzi, Stealth and cationic nanoliposomes as drug delivery systems to increase andrographolide BBB permeability, Pharmaceutics 10 (2018) 128, https://doi.org/10.3390/pharmaceutics10030128.
[34] G. Faraco, M. Pittelli, L. Cavone, S. Fossati, M. Porcu, P. Mascagni, G. Fossati, F. Moroni, A. Chiarugi, Histone deacetylase (HDAC) inhibitors reduce the glial inflammatory response in vitro and in vivo, Neurobiol. Dis. 36 (2009) 269–279, https://doi.org/10.1016/j.nbd.2009.07.019.

[35] Pellegrini-Giampietro Landucci, Bergonzi Bilia, Enhanced neuroprotective effects of Panax Ginseng G115® and Ginkgo Biloba GK501® combinations in vitro models of excitotoxicity, Int. J. Mol. Sci. 20 (2019) 5872, https://doi.org/10.3390/ijms20235872.
[36] L. Marques, A.A. Johnson, A. Stolzing, Doxorubicin generates senescent microglia that exhibit altered proteomes, higher levels of cytokine secretion, and a decreased ability to internalize amyloid β, Exp. Cell Res. 395 (2020) 112203 https://doi.org/10.1016/j.yexcr.2020.112203.
[37] M. Marques, L. de S. Hayashide, P. Amorim, B.M. Fernandes, A.P.B. Araujo, D. F. Messor, V.E. Leocadio, B. Pessoa, J.B.L.P. Corrêa, C. Villablanca, R.L. Vidal, C. González-Billault, I. Matias, F.C.A. Gomes, L.P. Diniz, Doxorubicin induces a senescent phenotype in Murine and human astrocytes, J. Neurochem. 169 (2025) e70177, https://doi.org/10.1111/jnc.70177.
[38] L. Zhang, L.E. Pitcher, M.J. Yousefzadeh, L.J. Niedernhofer, P.D. Robbins, Y. Zhu, Cellular senescence: a key therapeutic target in aging and diseases, J. Clin. Investig. 132 (2022), https://doi.org/10.1172/JCI158450.
[39] V. Lucas, C. Cavadas, C.A. Aveleira, Cellular senescence: from mechanisms to current biomarkers and senotherapies, Pharmacol. Rev. 75 (2023) 675–713, https://doi.org/10.1124/pharmrev.122.000622.
[40] L. Roger, F. Tomas, V. Gire, U. Galderisi, G. Di Bernardo, Mechanisms and regulation of cellular senescence, Int. J. Mol. Sci. 22 (2021) 13173, https://doi.org/10.3390/ijms222313173, 22 (2021) 13173.
[41] E. Csekes, L. Račková, Skin aging, cellular senescence and natural polyphenols, Int. J. Mol. Sci. 22 (2021) 12641, https://doi.org/10.3390/ijms222312641, 22 (2021) 12641.
[42] M. Baeeri, S. Momtaz, M. Navaei-Nigjeh, K. Niaz, M. Rahimifard, S.F. Ghasemi-Niri, N. Sanadgol, M. Hodjat, M. Sharifzadeh, M. Abdollahi, Molecular evidence on the protective effect of ellagic acid on phosalone-induced senescence in rat embryonic fibroblast cells, Food Chem. Toxicol. 100 (2017) 8–23, https://doi.org/10.1016/j.fct.2016.12.008.
[43] C. Ceci, G. Graziani, I. Faraoni, I. Cacciotti, Strategies to improve ellagic acid bioavailability: from natural or semisynthetic derivatives to nanotechnological approaches based on innovative carriers, Nanotechnology 31 (2020) 382001, https://doi.org/10.1088/1361-6528/ab912c.
[44] N. Stojiljković, S. Ilić, N. Stojanović, L. Janković-Veličković, S. Stojnev, G. Kocić, G. Radenković, I. Arsić, M. Stojanović, M. Petković, Nanoliposome-encapsulated ellagic acid prevents cyclophosphamide-induced rat liver damage, Mol. Cell. Biochem. 458 (2019) 185–195, https://doi.org/10.1007/s11010-019-03541-8.
[45] P. Patel, A. Thanki, D.U. Kapoor, B.G. Prajapati, QbD decorated ellagic acid loaded polymeric nanoparticles: factors influencing desolvation method and preliminary evaluations, Nano-Struct. Nano-Objects 40 (2024) 101378, https://doi.org/10.1016/j.nanoso.2024.101378.
[46] R. Reliene, A. Shirode, J. Coon, S. Nallanthighal, D. Bharali, S. Mousa, Nanoencapsulation of pomegranate bioactive compounds for breast cancer chemoprevention, Int. J. Nanomed. 10 (2015) 475, https://doi.org/10.2147/IJN.S65145.
[47] V. Arulmozhi, K. Pandian, S. Mirunalini, Ellagic acid encapsulated chitosan nanoparticles for drug delivery system in human oral cancer cell line (KB), Colloids Surf. B Biointerfaces 110 (2013) 313–320, https://doi.org/10.1016/j.colsurfb.2013.03.039.
[48] M.Y. Alfaifi, S.I. Elbehairi, A.A. Shati, U.A. Fahmy, N.A. Alhakamy, S. Md, Ellagic acid loaded TPGS micelles for enhanced anticancer activities in ovarian cancer, Int. J. Pharmacol. 16 (2019) 63–71, https://doi.org/10.3923/ijp.2020.63.71.
[49] K.S. Allemailem, Enhanced activity of Ellagic acid in lipid nanoparticles (EA-liposomes) against Acinetobacter baumannii in immunosuppressed mice, Saudi J. Biol. Sci. 30 (2023) 103707, https://doi.org/10.1016/j.sjbs.2023.103707.
[50] F. Heidarian, S.H. Alavizadeh, M.R. Kalantari, S.J. Hoseini, H.K. Farshchi, M. R. Jaafari, M. Doagooyan, A. Bemidinezhad, P. Kesharwani, A. Sahebkar, F. Gheybi, Ellagic acid nanoliposomes potentiate therapeutic effects of PEGylated liposomal doxorubicin in melanoma: an in vitro and in vivo study, J. Drug Deliv. Sci. Technol. 93 (2024) 105396, https://doi.org/10.1016/j.jddst.2024.105396.
[51] A. Agostini, L. Mondragõn, A. Bernardos, R. Martínez-Máñez, M. Dolores Marcos, F. Sancenõn, J. Soto, A. Costero, C. Manguan-García, R. Perona, M. Moreno-Torres, R. Aparicio-Sanchis, J.R. Murguía, Targeted cargo delivery in senescent cells using capped mesoporous silica nanoparticles, Angew. Chem. Int. Ed. 51 (2012) 10556–10560, https://doi.org/10.1002/anie.201204663.
[52] H. Jiang, Z.-P. Li, G.-X. Tian, R.-Y. Pan, C.-M. Xu, B. Zhang, J.-L. Wu, Liver-targeted liposomes for codelivery of curcumin and combretastatin A4 phosphate: preparation, characterization, and antitumor effects, Int. J. Nanomed. 14 (2019) 1789–1804, https://doi.org/10.2147/IJN.S188971.
[53] B. Lian, H. Wei, R. Pan, J. Sun, B. Zhang, J. Wu, X. Li, G. Tian, Galactose modified liposomes for effective Co-Delivery of Doxorubicin and combretastatin A4, Int. J. Nanomed. 16 (2021) 457–467, https://doi.org/10.2147/IJN.S283793.
[54] M. Kim, S. Bin Kim, J. Kim, K.S. Kim, D.E. Kim, Co-delivery of curcumin and PTTG1 siRNA by galactose receptor-targeted liposomes for enhanced anti-tumor effects in hepatocellular carcinoma, J. Drug Deliv. Sci. Technol. 86 (2023) 104692, https://doi.org/10.1016/j.jddst.2023.104692.
[55] M. Lafuente-Merchan, S. Ruiz-Alonso, A. Espona-Noguera, P. Galvez-Martin, E. López-Ruiz, J.A. Marchal, M.L. López-Donaire, A. Zabala, J. Ciriza, L. Saenz-Del-Burgo, J.L. Pedraz, Development, characterization and sterilisation of Nanocellulose-alginate-(hyaluronic acid)- bioinks and 3D bioprinted scaffolds for tissue engineering, Mater. Sci. Eng., C 126 (2021) 112160, https://doi.org/10.1016/j.msec.2021.112160.
[56] T. Hernández-Caselles, J. Villalaín, J.C. Gómez-Fernández, Influence of liposome charge and composition on their interaction with human blood serum proteins, Mol. Cell. Biochem. 120 (1993) 119–126, https://doi.org/10.1007/BF00926084.
[57] L.A. Fiel, K. Paese, M. Rizzi, S.S. Guterres, A.R. Pohlmann, A strategy to estimate the intrinsic flux of a poorly water soluble substance for comparison with its release from lipid-core nanocapsules, Colloids Surfaces A Physicochem. Eng. Asp. 441 (2014) 716–724, https://doi.org/10.1016/j.colsurfa.2013.10.036.
[58] L. de S. Teixeira, T.V. Chagas, A. Alonso, I. Gonzalez-alvarez, M. Bermejo, J. Polli, K.R. Rezende, Biomimetic artificial membrane permeability assay over franz cell apparatus using BCS model drugs, Pharm. Times 12 (2020) 988, https://doi.org/10.3390/PHARMACEUTICS12100988. Page 988 12 (2020).
[59] X. Mao, L.F. Wu, H.J. Zhao, W.Y. Liang, W.J. Chen, S.X. Han, Q. Qi, Y.P. Cui, S. Li, G.H. Yang, Y.Y. Shao, D. Zhu, R.F. Wang, Y. You, L.Z. Zhang, Transport of corilagin, gallic acid, and ellagic acid from fructus phyllanthi tannin fraction in Caco-2 cell monolayers, Evid. Based Complement. Alternat. Med. 2016 (2016) 9205379, https://doi.org/10.1155/2016/9205379.
[60] A. González-Sarrías, M.Á. Núñez-Sánchez, J. Tomé-Carneiro, F.A. Tomás-Barberán, M.T. García-Conesa, J.C. Espín, Comprehensive characterization of the effects of ellagic acid and urolithins on colorectal cancer and key-associated molecular hallmarks: MicroRNA cell specific induction of CDKN1A (p21) as a common mechanism involved, Mol. Nutr. Food Res. 60 (2016) 701–716, https://doi.org/10.1002/mnfr.201500780.
[61] C. Ceci, P.M. Lacal, L. Tentori, M.G. De Martino, R. Miano, G. Graziani, Experimental evidence of the antitumor, antimetastatic and antiangiogenic activity of ellagic acid, Nutrients 10 (2018) 1756, https://doi.org/10.3390/nu10111756.
[62] A. Gupta, A.K. Pandey, Aceclofenac-induced hepatotoxicity: an ameliorative effect of Terminalia bellirica fruit and ellagic acid, World J. Hepatol. 12 (2020) 949–964, https://doi.org/10.4254/wjh.v12.i11.949.
[63] D.D. Evtyugin, S. Magina, D.V. Evtuguin, Recent advances in the production and applications of ellagic acid and its derivatives. A review, Molecules 25 (2020), https://doi.org/10.3390/molecules25122745.
[64] V. Baradaran Rahimi, M. Ghadiri, M. Ramezani, V.R. Askari, Antiinflammatory and anti-cancer activities of pomegranate and its constituent, ellagic acid: evidence from cellular, animal, and clinical studies, Phytother Res. 34 (2020) 685–720, https://doi.org/10.1002/ptr.6565.
[65] V.B. Rahimi, V.R. Askari, S.H. Mousavi, Ellagic acid reveals promising anti-aging effects against D-galactose-induced aging on human neuroblastoma cell line, SH-SY5Y: a mechanistic study, Biomed. Pharmacother. 108 (2018) 1712–1724, https://doi.org/10.1016/j.biopha.2018.10.024.
[66] E.N. Ismail, I. Jantan, S. Vidyadaran, J.A. Jamal, N. Azmi, Phyllanthus amarus prevents LPS-mediated BV2 microglial activation via MyD88 and NF-κB signaling pathways, BMC Complement. Med. Ther. 20 (2020) 202, https://doi.org/10.1186/s12906-020-02961-0.
[67] C.F. Alfredsson, F. Rendel, Q.L. Liang, B.E. Sundström, E. Nånberg, Altered sensitivity to ellagic acid in neuroblastoma cells undergoing differentiation with 12-O-tetradecanoylphorbol-13-acetate and all-trans retinoic acid, Biomed. Pharmacother. 76 (2015) 39–45, https://doi.org/10.1016/j.biopha.2015.10.008.
[68] C.S. Yang, B.C. Tzou, Y.P. Liu, M.J. Tsai, S.K. Shyue, S.F. Tzeng, Inhibition of cadmium-induced oxidative injury in rat primary astrocytes by the addition of antioxidants and the reduction of intracellular calcium, J. Cell. Biochem. 103 (2008) 825–834, https://doi.org/10.1002/jcb.21452.
[69] H.A. Rizk, M.A. Masoud, O.W. Maher, Prophylactic effects of ellagic acid and rosmarinic acid on doxorubicin-induced neurotoxicity in rats, J. Biochem. Mol. Toxicol. 31 (2017), https://doi.org/10.1002/jbt.21977.
[70] E. Bientinesi, M. Lulli, M. Becatti, S. Ristori, F. Margheri, D. Monti, Doxorubicin-induced senescence in normal fibroblasts promotes in vitro tumour cell growth and invasiveness: the role of Quercetin in modulating these processes, Mech. Ageing Dev. 206 (2022), https://doi.org/10.1016/j.mad.2022.111689.
[71] A. Bielak-Zmijewska, M. Wnuk, D. Przybylska, W. Grabowska, A. Lewinska, O. Alster, Z. Korwek, A. Cmoch, A. Myszka, S. Pikula, G. Mosieniak, E. Sikora, A comparison of replicative senescence and doxorubicin-induced premature senescence of vascular smooth muscle cells isolated from human aorta, Biogerontology 15 (2014) 47–64, https://doi.org/10.1007/s10522-013-9477-9.
[72] V. Kirsch, J.-M. Ramge, A. Schoppa, A. Ignatius, J. Riegger, In vitro characterization of doxorubicin-mediated stress-induced premature senescence in human chondrocytes, Cells 11 (2022) 1106, https://doi.org/10.3390/cells11071106.
[73] R. Kumari, P. Jat, Mechanisms of cellular senescence: cell cycle arrest and senescence associated secretory phenotype, Front. Cell Dev. Biol. 9 (2021) 645593, https://doi.org/10.3389/fcell.2021.645593.
[74] D. Berardi, Y. Hunter, L. van den Driest, G. Farrell, N.J.W. Rattray, Z. Rattray, The differential metabolic signature of breast cancer cellular response to olaparib treatment, Cancers (Basel) 14 (2022) 3661, https://doi.org/10.3390/cancers14153661.
[75] X. Sun, P.D. Kaufman, Ki-67: more than a proliferation marker, Chromosoma 127 (2018) 175–186, https://doi.org/10.1007/s00412-018-0659-8.
[76] F. D'Adda Di Fagagna, P.M. Reaper, L. Clay-Farrace, H. Fiegler, P. Carr, T. Von Zglinicki, G. Saretzki, N.P. Carter, S.P. Jackson, A DNA damage checkpoint

response in telomere-initiated senescence, Nature 426 (2003) 194–198, https://doi.org/10.1038/nature02118.
[77] V. Gorgoulis, P.D. Adams, A. Alimonti, D.C. Bennett, O. Bischof, C. Bishop, J. Campisi, M. Collado, K. Evangelou, G. Ferbeyre, J. Gil, E. Hara, V. Krizhanovsky, D. Jurk, A.B. Maier, M. Narita, L. Niedernhofer, J.F. Passos, P.D. Robbins, C. A. Schmitt, J. Sedivy, K. Vougas, T. von Zglinicki, D. Zhou, M. Serrano, M. Demaria, Cellular senescence: defining a path forward, Cell 179 (2019) 813–827, https://doi.org/10.1016/j.cell.2019.10.005.
[78] L.S. Melo Dos Santos, M. Trombetta-Lima, B. Eggen, M. Demaria, Cellular senescence in brain aging and neurodegeneration, Ageing Res. Rev. 93 (2024) 102141, https://doi.org/10.1016/j.arr.2023.102141.
[79] J. Wu, N. Dongzhu, C. Zhao, J. Liang, N. Wang, D. Suonan, S. Sun, Multi-target botanical complex attenuates cellular senescence via bidirectional P21/P53/SIRT1 regulation: dual model validation, Int. J. Mol. Sci. 26 (2025) 11394, https://doi.org/10.3390/IJMS262311394, 26 (2025) 11394.